Bio-Inspired Walking for Humanoid Robots Using Feet with Human-Like Compliance and Neuromuscular Control

Luca Colasanto[1], Nicolas Van der Noot[1,2] and Auke J. Ijspeert[1]

Abstract— The human foot plays a key role in human walking providing, among others, body support and propulsion, stability of the movement and impact absorption. These fundamental functionalities are accomplished by an extraordinarily rich bio-mechanical design. Nonetheless, humanoid robots follow different approaches to walk, hence, they generally implement rigid feet. In this study, we target the gap existing between the human foot and traditional humanoid-robot feet. More specifically, we evaluate the resulting advantages and drawbacks by implementing on a humanoid robot some of the properties and functionalities embedded in the human foot. To this end, we extract the physical characteristics of a prosthetic foot to develop a human-like foot model. This foot model is systematically tested in simulation in human-like walking tasks on flat ground and on uneven terrain. The movement of the limbs is generated by a muscle-reflex controller based on a simplified model of the human limbs. The gait features and the walking stability are evaluated for the human-like foot and compared with the results produced using rigid feet.

I. INTRODUCTION

Comparing human and humanoid robot locomotion rises many questions about what is missing in these machines to achieve a proper human-like walk. In fact, most of the humanoid robots walk with bended knees and feet kept parallel to the ground, hence, they are limited in step length and they lack in robustness when subject to environmental disturbances. These questions have many possible answers concerning the differences in cognition capabilities, control strategies and mechanical properties. In this study, we focus on the big gap existing between the human foot and the traditional solutions used in humanoid robotics.

The human foot has a very complex structure composed of more than 100 muscles and tendons interconnecting 26 bones and a total number of almost 30 joints [1]. Such a rich bio-mechanical design gives to the foot many interesting properties and functionalities. For instance, the shape and the mobility of the bones of the foot play a key role absorbing internal and external impacts [2]. Moreover, the soft tissues of the plantar arch contribute to absorb external impacts and damp out vibrations. Finally, the Windlass mechanism [1] (a passive mechanism embedded in the foot) prevents the plantar arch to collapse under the body weight. Moreover, it kinematically constrains the toes-flexion and plantar-flexion. Therefore, it contracts the foot arch when the foot rolls over the toes.
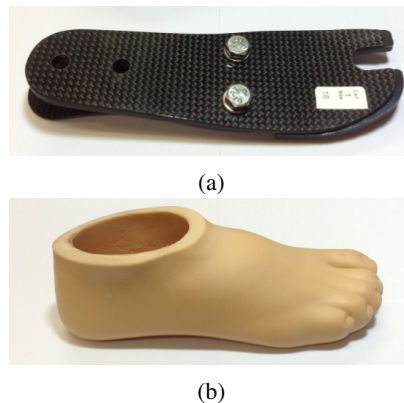
[1]Biorobotics Laboratory, EPFL, Lausanne, Switzerland
[2]Center for Research in Energy and Mechatronics, Université catholique de Louvain, Belgium

(a)

(b)

Fig. 1: (a) the Flex-Foot® Junior prosthesis; (b) the cosmetic cover

On the contrary, most humanoid robots, existing nowadays, are equipped with rigid and flat feet. As a consequence, the control efforts to achieve stable walking lie entirely on the upper body. This results, generally, in a very unnatural walk. Nevertheless, more advanced feet for humanoid robots already exist. A common practice to increase the shock absorbance at the lover-limb extremities consists in adding soft material (for instance rubber) under the sole of the foot of the robot [3]. Example of multi-body foot design are, among others, reported in [4], [5], and [6]. Unfortunately, these more complex designs are still not explored on real humanoid robots. In fact, the most used walking strategies rely on the computation of dynamic stability indicators (such as the Zero-Moment Point [7]) that suppose to have the foot flat on the ground during the whole stance phase.

Passive prosthetic feet for amputees are developed to allow the user to walk comfortably at a specific nominal speed. In fact, they are designed to replicate the functionalities of the human foot introduced beforehand and to reproduce a similar behaviour. Fig. 1a depicts the Flex-Foot® Junior prosthesis. It is composed of two carbon fiber elements (a long element and a smaller one) connected in the middle by two screws. The overall shape appears similar to the shape of the human foot having the heel, forefoot, foot tomb and the plantar arch. However, the similarity is also functional. In fact, pressing on the foot tomb, the longer element bends pushing down the heel. It is similar to what happens on the human foot due to the Windlass mechanism. Moreover, the round shape and the stiffness of the heel and the foot toes are selected to have a proper foot-roll movement during the walk. The cosmetic

cover, in Fig. 1b, is used to allow the prosthesis to wear normal shoes. However, it also adds extra compliance at the heel and the foot toes and increases the impulse absorption, similarly to the soft tissues of the human foot.

The motivation of this study comes from the wish to quantify the benefits that can be obtained by using more human-like foot designs in humanoid robotics. To this end, we extract the physical characteristics of a prosthetic foot to develop a human-like foot model. In [8], the authors characterized the physical properties of the human foot measuring them directly on an amputated foot. More recently, in [9], the authors measured the kinematic of the bones in an amputated foot while performing a walking gait. In our approach, we use a commercial prosthesis instead of directly analyzing the human foot. This solution has many advantages. Among others, we inherit the knowledge of prosthetic manufacture in the design of a device reproducing the main features of a human foot and we produce data which are reproducible in any other lab. However, the characteristics of the passive prosthesis are fixed and cannot be adapted to different gaits. In [10], we achieved human-like walking using neuromechanical primitives. More specifically, the walking controller is based on a set of virtual muscles activated by reflexes. Exploiting the principles of legged mechanics and muscle activations, the robot was able to walk on flat ground, exhibiting some human-like features as stretched stance leg and rolling feet. In this study, we use a similar muscle-reflex based controller together with the human-like foot. We optimize several walking gaits on a wide range of walking speeds. Respect to previous attempts to achieve human like walking using flexible feet, such as [11] and [12], we are able to reach higher walking speeds. Our walking strategy is systematically tested on flat ground and uneven terrain to evaluate the walking efficiency and robustness. In [13], the authors conduct a similar study producing interesting results on the energy consumption of a compliant foot. Our analysis focuses not only on the energy but also on other gait features and fundamental aspects of walking such as terrain adaptation. Finally, we compare the results obtained using human-like compliant feet with the ones obtained using rigid feet.

In the following Section, the foot designs are presented. In Sec. III, the principles of the muscle-reflex controller are explained. More details on the optimization process and the different scenarios used to evaluate the foot designs are collected in Sec. IV. Finally, the results are reported and discussed in Sec. V and VI.

II. Foot Models

For the purposes of this study, we extract the physical characteristic of a prosthetic foot to develop a human-like foot model. Beside, two variations of the rigid foot are proposed and used as benchmark in the performance evaluation. In this Section, the three foot designs are described.
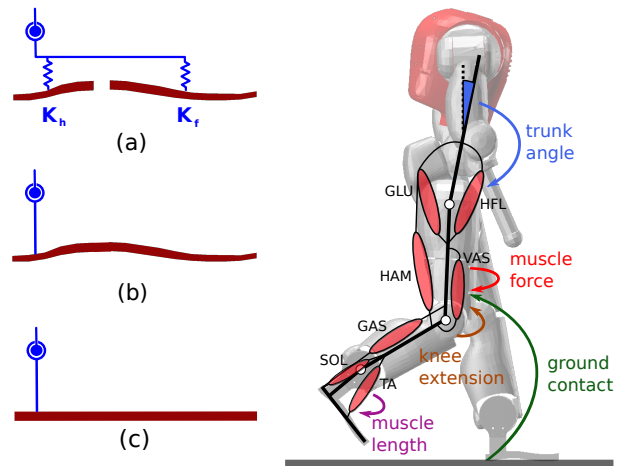

Fig. 2: Left panel: Three foot designs: (a) the human-like foot; (b) the rigid-shaped foot; (c) the rigid-flat foot. Right panel: COMAN robot with the seven muscle groups of the right leg and some inputs of the controller reflex rules. Muscles: soleus (SOL), tibialis anterior (TA), gastrocnemius (GAS), vasti (VAS), biarticular hamstring (HAM), gluteus (GLU) and hip flexor (HFL).

A. The Human-Like Foot

The dual-profile prosthetic design, of the selected prosthesis, is one of the most common among passive prosthetic devices. It is well known in the prosthetic scientific community as well. Hence, it allowed us to study the design strategy behind it. More specifically, the Flex-Foot® Junior, produced by Össur ehf, is available in three different versions according to the weight of the patient and in different sizes according to the body of the patient. Considering the 30 kg of mass and the 5-years-old body proportion of our robot, COMAN [14], the Flex-Foot® Junior is the most appropriate commercial prosthesis available on the market.

The prosthesis interacts with the ground in three different configurations during a step. At the heel-strike, just the hindfoot is touching the ground, hence, the heel profile bends and adapts to the terrain. The force (F_h) that the hindfoot exhibits, strictly depends on this deflection. At the toe-off, just the forefoot is in contact with the ground, and then it bends. The force exerted (F_f) mainly depends on the corresponding deflection. During the stance phase, both parts (the hindfoot and the forefoot) are in contact. Hence, the total force exerted is equal to $F_h + F_f$.

A schematic of the model used to represent this behavior is depicted in Fig. 2a. K_h and K_f are respectively the vertical heel stiffness and the vertical forefoot stiffness assumed non linear. Hence, the vertical forces exerted at the hindfoot and forefoot can be expressed as follows:

$$f_h = K_h(\delta_h)\delta_h \qquad f_f = K_f(\delta_f)\delta_f \qquad (1)$$

where δ_h and δ_f are respectively the heel deflection and the forefoot deflection of the two vertical springs. The red plates, attached to the springs (see Fig. 2a), are shaped as the real sole of the prosthetic foot. They are constrained horizontally, hence they can only move vertically according to the springs
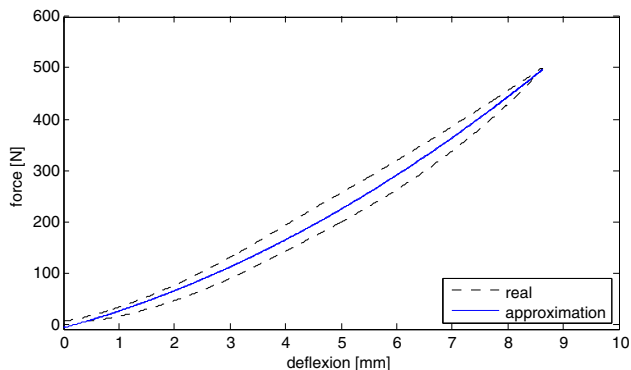
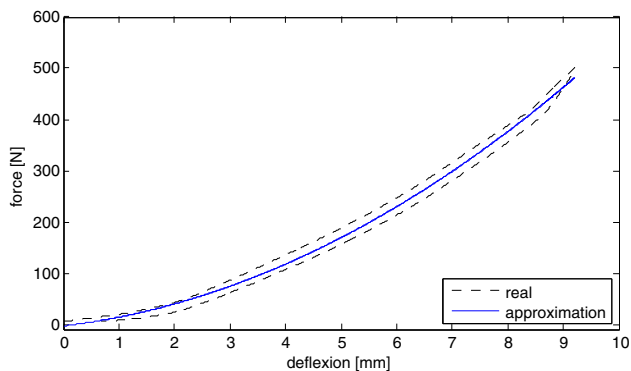Fig. 3: Force-displacement characteristic of the hindfoot

Fig. 4: Force-displacement characteristic of the forefoot

deflection (δ_h and δ_f) The sole profile is very important because it affects the motion of the center of pressure during the step. Hence, it affects the motion dynamics of the walker too. For instance, the curvature of the heel and the forefoot affects the foot roll movement during heel strike and toe off respectively. Moreover, having different values of stiffness for the hindfoot and the forefoot, affects the force distribution below the sole and moment at the ankle joint. The energy storage capability directly depends from those values as well.

In order to compute Eq. (1), we experimentally compute the functions $K_h(\delta_h)$ and $K_f(\delta_f)$. The plot in Fig. 3 collects the data relative to the heel. The quasi-static force-displacement characteristic of the heel is represented with a dotted black line. As expected, the characteristic is not linear. Moreover the compression characteristic differs from the extension characteristic, mostly due to the hysteresis properties of the cosmetic cover [15]. For the purposes of this study, we do not model the hysteresis of the prosthetic foot. In fact, rather than an highly accurate identification of this specific prosthesis, we are interested in capturing the general behaviour. Hence, we approximate this curve with a second-order polynomial function (represented with a solid blue line in the plot) using the least-squares algorithm. The heel stiffness $K_h(\delta_h)$ is approximated with the derivative of this function. In a similar way we compute the forefoot stiffness function $K_f(\delta_f)$. In Fig. 4, the quasi-static force-displacement characteristic of the forefoot is represented with

a dotted black line. This curve is similar to the one in Fig. 3. The second-order approximation of the characteristic is represented with a solid blue line.

In this study, we did not characterize the damping of the prosthetic foot. However, we apply low damping forces parallel to f_h and f_f and proportional to $-\dot{\delta}_h$ and $-\dot{\delta}_f$. The main reason is to guarantee the convergence of the sole plates to the equilibrium positions.

B. The Rigid feet

In Fig. 2c the first variant of the rigid foot is depicted: the Rigid Flat Foot (RFF). The sole of the foot (in red) is a single element completely rigid and its shape is flat. The total length and the position of the ankle joint are the same as the HLF.

The Rigid Shaped Foot (RSF) is depicted in Fig. 2b. It is an intermediate version between the HLF and the RFF. In fact, its sole is completely rigid but it has the same shape as the HLF. Proportions are the same of the other two feet.

III. The Muscle-Reflex based Controller

The bio-inspired controller presented in [16], achieves Limit Cycle Walking on a simplified model of a human. The locomotion is then entirely controlled by a chain of reflexes commanding human muscle groups. We implement a similar controller to get stable locomotion gaits on the COMAN. We focus on 2D walking gaits, hence, no motion is permitted in the lateral and transverse plane. Consequently, all robot non-sagittal Degrees Of Freedom (DOFs) are set to a fixed position. Compared to the simplified human model used in [16], we have extra DOFs for the upper body (controlled using the rules described in [17]). Moreover, we include the robot series-elastic-actuator dynamics [18] because we want to derive a controller that could be directly plugged into the real robot.

Seven muscle groups are identified within each leg, as depicted on the right side of Fig. 2. Each muscle group is represented by a Hill-type muscle, a set of equations developed to fit the behaviour of a real muscle. They are controlled by scalar signals: the neuronal stimulation signals, being generated by some reflex rules. These rules are a set of equations using different inputs: the trunk absolute angle, the ground contact forces, the knees position and the muscles length and force. These reflex rules require an optimization phase to find a set of unknown parameters, as described in Sec. IV-A.

The different virtual muscles react to the activation signals by contracting. The forces generated are mapped into the joint space considering the segments free-body diagram. Hence, the desired torques are sent as references to a low-level torque controller implemented as in [18]. Finally, the outputs of this low-level controller are used in the motor equations, generating the actual torques.

IV. Simulation Environment

The dynamical model of the COMAN robot is generated in Robotran [19]-[20]. It is a software able to model and analyze

(a) heel-strike   (b) toe-off   (c) single-support   (d) heel-strike
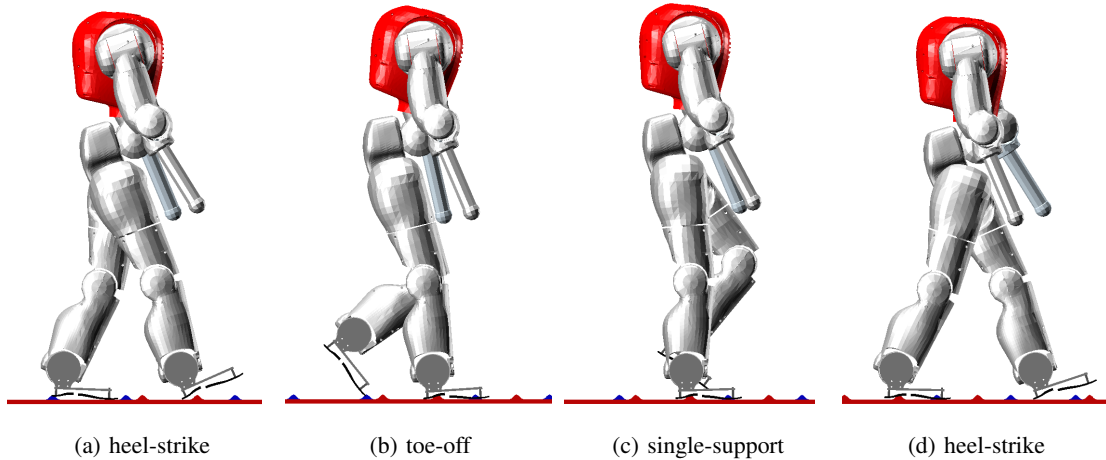
Fig. 5: Snapshots of the COMAN walking on uneven terrain. Blue bumps affect the left foot and red bumps affect the right one.
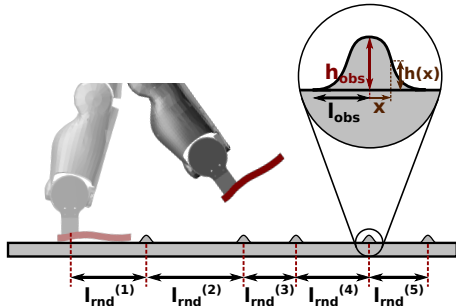

Fig. 6: Uneven terrain profile.

multibody systems. On top of the robot body dynamics, its actuator dynamics is implemented as described in Section III and different feet designs are implemented as presented in Sec. II.

To fully present the simulation environment, we first detail the controller optimization phase and finally, we introduce the different scenarios used to compare the different feet design performances.

A. The Gait Optimization

The muscle-reflex based controller involves a set of unknown parameters that must be tuned with an optimization phase. These parameters directly impact the features of the robot gait, among others, its speed and energy consumption. We aim to compare different foot designs. To this end, we only compare gaits with the same speed. Consequently, getting a final target speed is one of the requirements of the optimization. We also want the controllers to be energetically efficient. To get more human-like walkers, we aim to minimize the metabolic energy consumption in the virtual muscles per unit distance walked [21].

The selected optimization algorithm is a heuristic one called *Particle Swarm Optimization* [22] [23]. To achieve all the above-mentioned requirements, each set of parameters is tested according to a staged objective function. This means that the different objectives are sorted by order of relevance

so that the next objective is taken into account (in the objective function) only when the previous one is fulfilled.

The first stage rewards the gait robustness, by assigning an objective function proportional to the walking time (before a possible fall). A fitness of 100 is assigned to a non falling walk of $60\,\mathrm{s}$. To further improve the gait robustness, we want the robot to keep a foot clearance of at least $1\,\mathrm{cm}$ above the ground when walking on a flat surface.

When the COMAN is able to walk without falling during the entire simulation time (i.e. $60\,\mathrm{s}$), the second stage of the objective function is unlocked. This one constrains the gait to achieve a target speed. Different target speeds are tested ranging from $0.4\,m/s$ to $0.9\,m/s$, which covers the normal walking speed range for a five-years-old child. The objective function f is computed as follows:

$$f = \alpha \, e^{-\beta \, (x-x^*)^2} \tag{2}$$

where x is the forward speed, x^* the target speed and α, β two weight parameters ($\alpha = \beta = 100$). Hence, this function is bounded between 0 and α.

If the robot speed lies within an interval of $0.05\,\mathrm{m/s}$ around the target speed, the last stage is unlocked, i.e. the energy minimization. The objective function is formulated as Eq. (2). However, x^* is set to zero while x is now the metabolic energy consumption per unit distance walked and per mass unit ($\alpha = 100$ and $\beta = 5 \cdot 10^{-6}$). This helps minimizing the absolute energy expenditure.

B. Optimization and Evaluation Senarios

To evaluate the feet designs or to optimize their respective controllers, we use different types of ground. The property of the contact model are the same , however, the ground profile changes to fulfil different requirements. Referring to Fig. 6, we define the following ground profiles:

(a) *Flat ground:* This ground is totally flat with no obstacles and is used to evaluate the different gait features: energy consumption, stride length and stride frequency.

(b) *Uneven terrain:* In order to evaluate the contribution of the different foot designs to the walking stability, we use a flat ground with small bumps. Referring to Fig. 6, the shape of the bumps can be computed as follows:

$$h(x) = \frac{h_{obs}}{2} \left(1 + cos \left(\frac{\pi}{l_{obs}} x \right) \right) \qquad (3)$$

where h_{obs} and $l_{obs} = 1.5cm$ are respectively the total height and the half of the base length of the bump. Using this sinusoidal shape, there is no slope discontinuity in the ground contact model. The distance between two consecutive bumps (l_{rnd}) is randomly computed with a flat distribution bounded between $100\,mm$ and $200\,mm$. Consequently, the feet ($150\,mm$ long) can land on a perfectly flat terrain or on a location with one or two bumps.

Finally, we prevent the robot from falling due to a collision between the toes of the swing foot and a bump. Hence, we make these bumps to only interfere with a landing foot (and during the stance phase). This does not constitute a loss of generality, for the purposes of this study (see Sec. VI).

V. RESULTS

For each foot design and for each target speed, we run five optimizations (with different random initial populations) that converge to as many sets of controller parameters that allow the COMAN to walk at the requested speed on the flat ground for at least $60s$.

Snapshots of the resulting walking gait are presented in Fig. 5. The COMAN performs the heel-strike with its right foot. Meanwhile the left foot rolls over the toe and swings in front of the opposite leg. The supporting leg propels the body forward and the corresponding foot adapts to the uneven ground. The next step starts with the heel-strike of the left foot.

The gait features and walking stability of these controllers with the corresponding foot designs are evaluated in the next Section.
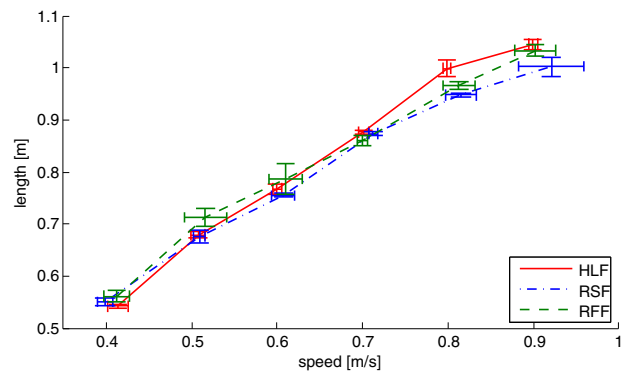
A. Gait features

The plot in Fig. 7a collects the values of the energy consumption measured during an eight-meter steady-state walk on flat ground. The data corresponding to the HLF are represented in red and the data corresponding to the RSF and RFF are represented respectively in blue and green. For each target speed and each foot design, we summarize the five optimized controllers by presenting the mean and the standard deviations of their characteristics. The energy values for the two variants of the rigid foot are very close to one another at low speed and slowly diverge at high speed maintaining the same trend. The minimum energy value corresponds to speeds of $0.8154m/s$ and $0.8126m/s$ respectively for RSF and RFF. The rigid human-like shape of the sole lower the energy efficiency of the RSF respect to RFF. The HLF has higher energy consumption for the whole speed range, and has its lowest values between $0.5073m/s$
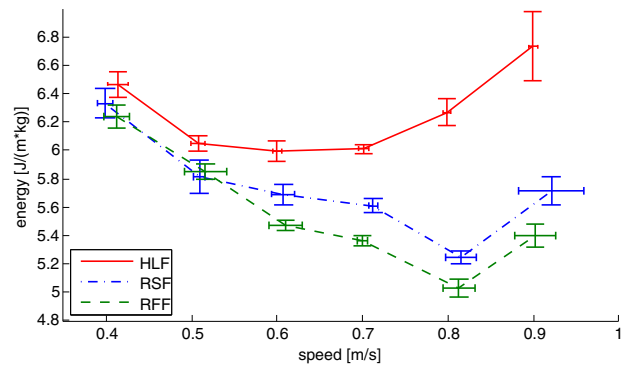
(a) Energy consumption per mass unit and per unit distance walked
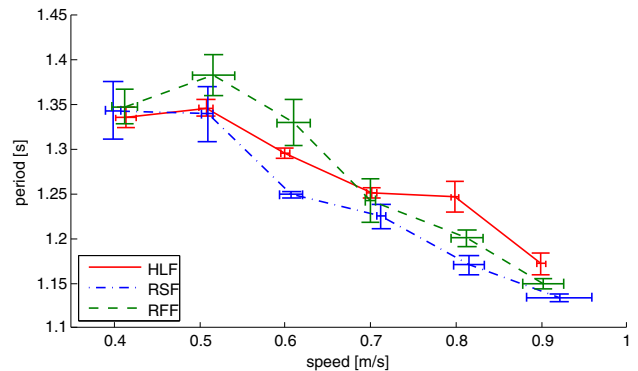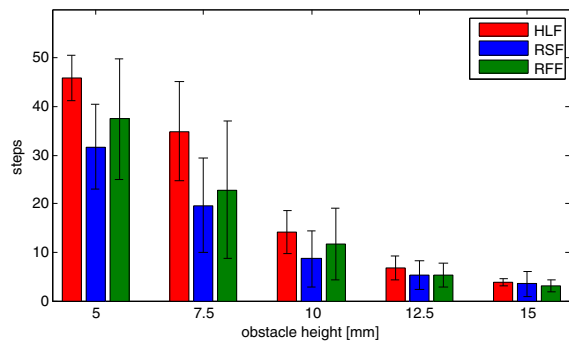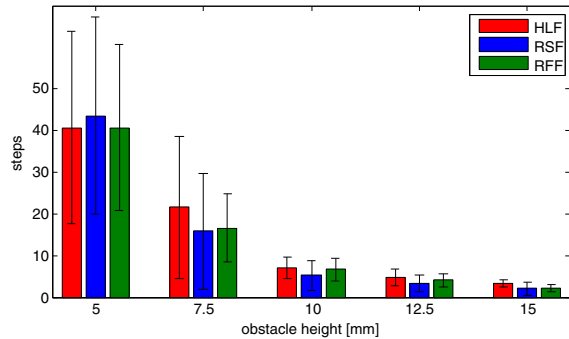

(b) Stride period

(c) Stride length

Fig. 7: Mean value and standard deviation of the gait features for the different walking speeds and the different foot designs : Human-Like Foot (HLF), Rigid Shaped Foot (RSF), Rigid Flat Foot (RFF).

and $0.706m/s$. Moreover, its standard deviation regularly increase for high speed, demonstrating a higher variability of the controller parameters.

The plots in 7b and 7c collect respectively the values of the stride duration and the stride length during the walk. As for Fig. 7a, we present their mean values and the standard deviations. Their trends are mostly monotonic with respect to the walking speed and they are slightly affected by the foot design. The rigid human-like shape of the sole of RSF induces a lower walking frequency and longer stride compared to RFF at any speed. The trend of the walking frequency for the HLF is more flat along the whole speed

(a)

(b)

Fig. 8: Endurance test results for different walking speed : (a) 0.5 m/s ; (b) 0.8 m/s

Fig. 9: Snapshots of the real COMAN walk. The robot is constrained on the sagittal plane by its hands.

range. Hence, its stride length compared with the two rigid designs is slightly smaller at lower speed and bigger at high speed.

B. Walking Stability

The influence of the foot designs to the robustness of walking is evaluated by an endurance test on uneven terrains. More specifically, the COMAN has to blindly walk on different uneven terrains with different obstacle heights (see Fig. 6). Hence, the three foot designs are tested on the same terrain conditions and the number of steps performed before falling are considered as index of walking stability. It is important to remark that the controllers are optimized on flat ground (see Sec.IV-B). Therefore, the difference in the number of steps performed are related to the different features of the feet rather than the controller.

The chart in Fig. 8a collects the results of the endurance tests performed using the controllers optimized for a speed equal to $0.5m/s$. This is the limit value of the speed range (between $0.5m/s$ and $0.7m/s$) having the most efficient gaits on flat ground for the HLF (see Fig.7a). For each bump height, the number of steps performed before falling are represented with a red, blue and green bar respectively for the HLF, the RSF and the RFF. The standard deviations are reported too. The HLF results to be the most stable along the whole observed range. The RSF and RFF present very
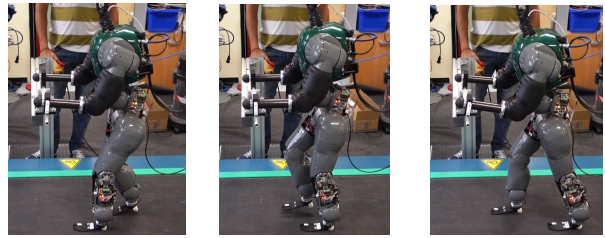
similar results for bump heights bigger than $1cm$.

The chart in Fig. 8b, collects the results of the endurance tests performed at the most efficient gait on flat ground for the rigid feet : $0.8m/s$ (see Fig.7a). The advantage of HLF on the rigid feet is much reduced respect to results of Fig. 8a.

VI. CONCLUSIONS AND FUTURE WORK

In this work, we investigated the advantages and the drawbacks of implementing human-like compliant feet to a humanoid robot driven by a neuromuscular controller.

The rigid foot results in more energy efficient gaits than the human-like foot. This characteristic is in line with the results presented in other work such as [13]. It has its minimum energy consumption for walking speed close to $0.8m/s$ and increases around it. The trend of the human-like design is similar and has its minimum energy between $0.5m/s$ and $0.7m/s$. In fact, this model is based on a passive prosthesis that is designed to match the human behaviour around a specific range of speeds (between $0.52m/s$ and $0.83m/s$ for a normal child [24]). Other gait features slightly differ. The shape of the sole affects the walking frequency at slow speed and the compliance mainly affects the straight length at high speed.

Despite its high energy consumption, the human-like foot has the best performance in terms of stability of the walking. The shape of the sole and the different compliance between the hindfoot and the forefoot probably increase the foot adaptability to the ground uncertainties and reject more efficiently the disturbances with respect to a rigid foot. The data reported in Fig. 8, refer to a blind walk and no strategies are implemented to guarantee robustness to ground perturbation. This leads to a minimization of the influence of the controller to the walking robustness, and therefore an unbiased evaluation of the performances of the different feet. By implementing extra stabilization strategies (such as stumbling reflexes) or optimizing the control parameters directly on rough terrains, the robustness of the walk could certainly be increased. However, the aim of this study is different.

The results of this study are promising. In fact, using human-like compliant feet together with the neuromuscular controller, we achieved walking gaits in a wide range of speed. Moreover, we showed an increase of robustness of the walk using soft feet respect to rigid ones. The obstacle

sizes and the walking speeds, considered in this study, were selecting according to the kid-size proportions of the COMAN robot. In order to compare these results with an adult-size robot, a factor of 2, at least, should be considered.

Our future work will be collecting experimental data with the real robot implementing the prosthetic feet. Snapshots of a preliminary test performed on the real COMAN are presented in Fig. 9. This result is obtained using the exact same controller parameters optimized in simulation. In fact, the simulation included full model of the robot dynamics in the sagittal plane, the actuator dynamics and a realistic contact model. Moreover we are interested to further extend the model of the human-like compliance foot and deeper study its effects on the walking gait. For instance, we will analyze how the gait characteristics change using stiffer prosthesis.

ACKNOWLEDGMENT

REFERENCES

[1] J. H. Hicks, "The mechanics of the foot," *Journal of anatomy*, vol. 88, pp. 25–30.1, 1954.

[2] J. H. Chung, B.-j. Yi, and C. S. Han, *Intelligent Mobility Playing the Role of Impulse*. Distributed Autonomous Robotic Systems 8, 2009.

[3] J. Li, Q. Huang, W. Zhang, Z. Yu, and K. Li, "Flexible foot design for a humanoid robot," in *Automation and Logistics, 2008. ICAL 2008. IEEE International Conference on*, Sept. 2008, pp. 1414–1419.

[4] H. Yang, M. Shuai, Z. Qiu, H. Wei, and Q. Zheng, "A novel design of flexible foot system for humanoid robot," in *Robotics, Automation and Mechatronics, 2008 IEEE Conference on*, 2008, pp. 824–828.

[5] J. T. Seo and B. J. Yi, "Modeling and analysis of a biomimetic foot mechanism," in *2009 IEEE/RSJ International Conference on Intelligent Robots and Systems, IROS 2009*, 2009, pp. 1472–1477.

[6] S. Davis and D. G. Caldwell, "The design of an anthropomorphic dexterous humanoid foot," in *IEEE/RSJ 2010 International Conference on Intelligent Robots and Systems, IROS 2010 - Conference Proceedings*, 2010, pp. 2200–2205.

[7] M. Vukobratović and B. Borovac, "Zero-Moment Point - Thirty five years of its life," *International Journal of Humanoid Robotics*, vol. 01, no. 01, pp. 157–173, Mar. 2004. [Online]. Available: http://www.worldscientific.com/doi/abs/10.1142/S0219843604000083

[8] R. F. Ker, M. B. Bennett, S. R. Bibby, R. C. Kester, and R. M. N. Alexander, "The spring in the arch of the human foot," *Nature*, vol. 325, pp. 147–149, 1987.

[9] K. Ito, N. Ogihara, K. Hosoda, S. Shimizu, Kume, T. Nagura, T. Nakamura, N. Imanishi, S. Aiso, and M. N., Jinzaki, "Direct assessment of foot kinematics during human gait using a dynamic cadaver simulator and a biplane X-ray fluoroscopy," *Journal of Foot and Ankle Research*, vol. 7(Suppl 1), 2014.

[10] N. Van der Noot, L. Colasanto, A. Barrea, J. Van den Kieboom, R. Ronsse, and A. Ijspeert, "Experimental validation of a bio-inspired controller for dynamic walking with a humanoid robot," in *Intelligent Robots and Systems (IROS), 2015 IEEE/RSJ International Conference on*, 2015.

[11] Y. Ogura, K. Shimomura, H. Kondo, A. Morishima, T. Okubo, S. Momoki, H. ok Lim, and A. Takanishi, "Human-like walking with knee stretched, heel-contact and toe-off motion by a humanoid robot," in *Intelligent Robots and Systems, 2006 IEEE/RSJ International Conference on*, Oct 2006, pp. 3976–3981.

[12] K. Hashimoto, Y. Takezaki, K. Hattori, H. Kondo, T. Takashima, H. ok Lim, and A. Takanishi, "A study of function of foot's medial longitudinal arch using biped humanoid robot," in *Intelligent Robots and Systems (IROS), 2010 IEEE/RSJ International Conference on*, Oct 2010, pp. 2206–2211.

[13] S. Song and H. Geyer, "The energetic cost of adaptive feet in walking," in *ROBIO'11*, 2011, pp. 1597–1602.

[14] N. G. Tsagarakis, S. Morfey, G. M. Cerda, Z. Li, and D. G. Caldwell., "COMAN a compliant humanoid: optimal joint stiffness tuning for modal frequency control," in *IEEE International Conference on Robotics and Automation, . Proceedings. ICRA '13.*, 2013.

[15] H. W. L. Van Jaarsveld, H. J. Grootenboer, J. De Vries, and H. F. J. M. Koopman, "Stiffness and hysteresis properties of some prosthetic feet," *Prosthetics and Orthotics International*, vol. 14, no. 3, pp. 117–124, 1990. [Online]. Available: http://informahealthcare.com/doi/abs/10.3109/03093649009080337

[16] H. Geyer and H. Herr, "A muscle-reflex model that encodes principles of legged mechanics produces human walking dynamics and muscle activities," *Neural Systems and Rehabilitation Engineering, IEEE Transactions on*, vol. 18, no. 3, pp. 263–273, 2010.

[17] J. M. Wang, S. R. Hamner, S. L. Delp, and V. Koltun, "Optimizing locomotion controllers using biologically-based actuators and objectives," *ACM Trans. Graph*, pp. 25–25, 2012. [Online]. Available: http://citeseerx.ist.psu.edu/viewdoc/summary?doi=10.1.1.374.4172

[18] M. Mosadeghzad, G. A. Medrano-Cerda, J. A. Saglia, N. G. Tsagarakis, and D. G. Caldwell, "Comparison of various active impedance control approaches, modeling, implementation, passivity, stability and trade-offs," in *2012 IEEE/ASME International Conference on Advanced Intelligent Mechatronics (AIM)*. IEEE, July 2012, pp. 342–348.

[19] H. Dallali, M. Mosadeghzad, G. A. Medrano-Cerda, N. Docquier, P. Kormushev, N. Tsagarakis, Z. Li, and D. Caldwell, "Development of a dynamic simulator for a compliant humanoid robot based on a symbolic multibody approach," in *2013 IEEE International Conference on Mechatronics (ICM)*. IEEE, Feb. 2013, pp. 598–603.

[20] J.-C. Samin and P. Fisette, *Symbolic Modeling of Multibody Systems*. Springer, 2004.

[21] L. J. Bhargava, M. G. Pandy, and F. C. Anderson, "A phenomenological model for estimating metabolic energy consumption in muscle contraction," *Journal of Biomechanics*, vol. 37, no. 1, pp. 81–88, Jan. 2004.

[22] M. Clerc and J. Kennedy, "The particle swarm - explosion, stability, and convergence in a multidimensional complex space," *IEEE Transactions on Evolutionary Computation*, vol. 6, no. 1, pp. 58–73, 2002.

[23] J. Kennedy and R. Eberhart, "Particle swarm optimization," in *Proceedings of ICNN'95 - International Conference on Neural Networks*, vol. 4. IEEE, 1995, pp. 1942–1948.

[24] R. Rose-jacobs, "Development of Gait at Slow , Free , and Fast Speeds in 3- and 5-Year-Old Children," vol. 63, no. 8, pp. 1251–1259, 1983.